Title

SEAM WELD SCRAP REDUCTION IN PORTHOLE-DIE EXTRUSION OF 6XXX SERIES ALUMINUM ALLOYS USING A NOVEL PHYSICAL SIMULATION METHOD

Authors & Affiliations

Roni J. Rountree – Lehigh University, Bethlehem, PA
Charles Chemale Yurgel – Lehigh University, Bethlehem PA
Nicholas E. Nanninga – Secat Inc, Lexington KY
Randall Bowers – Secat Inc, University of Kentucky, Lexington KY
Paul F. Rottmann – University of Kentucky, Lexington KY
Wojciech Z. Misiolek – Lehigh University, Bethlehem PA

1. Abstract

Seam welds, essential for the direct extrusion of hollow aluminum profiles, contribute to substantial scrap that must be remelted, cast, and homogenized at high energy costs. These welds form in the solid state along the length of the extrudate, ideally yielding material properties similar to the bulk material by avoiding a heat-affected zone (HAZ) associated with the melting of the material. However, if bonding conditions are not correctly optimized, the seam weld can become a weak point in the extrudate, rendering it unsuitable for structural applications and contributing to scrap. Designing for proper bonding conditions in conjunction with other extrusion parameters presents a unique challenge to process design. While both physical and numerical simulation methods have been developed, they need to be improved in availability and practicality for industry application. To address this challenge, the presented research introduces a novel physical simulation approach to develop criteria for seam welds found in porthole-die extrusion of aluminum alloy 6005A and investigate the effect of varying deformation rate and temperature on the micro and macroscopic properties of the weld region. This technique involved using a Gleeble 3500 thermomechanical simulator to compress cylindrical blanks under isothermal conditions at different preheat temperatures and deformation rates. Flow stress responses were measured, and mechanical testing of the compressed blanks assessed bonding quality. Microstructural assessment (LOM, SEM, EBSD) was used to characterize bond quality and then correlated with the measured flow stress responses. This correlation successfully developed a weld criterion relating the bonding quality to the desired process parameters. These findings created a tool for aluminum extruders to develop their own seam weld criteria for a given set of process conditions using commercially available equipment. Additionally, the understanding of microstructural evolution responsible for solid-state bonding of aluminum was advanced. The development of this tool and understanding of solid-state bonding will enable the aluminum extrusion industry to reduce scrap and energy costs associated with seam weld defects. Future work will integrate this tool with numerical simulation using flow stress data from the Gleeble 3500 to model material plasticity under varying process conditions.

2. Introduction and Motivation

Demand for hollow aluminum extrudates in industries like construction, automotive, and aerospace is rising due to their strength, low weight, and recyclability. However, this increased demand also leads to higher energy use and carbon emissions from aluminum extrusion, making process optimization critical. Direct, porthole-die extrusion offers an efficient way to produce these extrudates, but seam weld defects can compromise their structural integrity [1]. In this process, material flow splits around bridges supporting a mandrel to define inner extrudate geometry, forming a seam weld upon rejoining. Seam welds form in solid-state, allowing for material properties close to the bulk material with careful control of temperature and deformation as the material is not liquified [2, 1]. However, the inability to optimize these solid-state bonding parameters can quickly reduce material properties in the seam weld resulting in extrudate scrap. Due to a lack of available predictive tools, this optimization is often performed using trial and error yielding high process scrap rates [3]. Thus, the need for predictive tools is crucial in reducing energy and emission burdens caused by seam weld scrap in porthole-die extrusion. The following work presents and evaluates a new method of physical simulation combined with numerical modeling to predict solid-state bonding behavior in seam welds in porthole die extrusion. This method uses uniaxial, isothermal, compression tests of two small, aluminum blanks to replicate deformation and temperatures found in porthole die extrusion of 6xxx series aluminum alloys. Numerical modeling by means of 2D finite element modeling (FEM) is used in conjunction with the physical simulation experiments for simultaneous quantification and prediction of solid-state bonding behavior. Corresponding weld behavior of the physical simulations is measured by means of micro tensile testing. A weld criterion based on the micro tensile results is developed to accept or reject seam welds by applying the criteria to local temperature and strain rate conditions withing the extrusion die based on FEM simulations. Later work will use the methods and results of this work to predict seam weld behavior in full scale porthole die extrusion of hollow, thick-walled, aluminum alloy extrudates.

3. Review of Related Work

Tools capable of predicting seam weld quality for porthole die extrusion primarily consist of simulation by means of physical and numerical modeling. Physical modeling refers to replicating metal forming processes physically in a small, laboratory setting whereas numerical modeling refers to using mathematical relationships and criteria to predict behavior in metal forming processes. Early physical models of extrusion consisted of wax, plasticine, or clay pushed through a modular die to predict flow patterns of the temperature softened metal such as work by Holmquist [4]. Physical modeling has become much more sophisticated than wax models and now consists of recreating metal flow found in extrusion using small, controlled experimentation. Physical modeling of this kind allows researchers to observe solid-state bonding mechanisms of seam welds in-situ while simultaneously recording data regarding these mechanisms. Chakkingal and Misiolek used physical modeling using a Gleeble thermomechanical simulator to investigate the mechanical strength of seam welds before and after heat treatment [5]. Elsewhere Edwards et al examined surface stretching effects on bond quality using a similar method [6]. Methods with instrumentation made in-house include efforts by Cooper and Allwood who replicated combined normal contact and shear stresses in solid-state bonding and Bai et al who recreated hydrostatic pressure inherent to porthole-die extrusion weld chambers [7, 8]. However, efforts simulating local isothermal conditions possible in weld chambers have yet to be made. Numerical modeling efforts in porthole die extrusion include both mathematical relationships and computer simulations using FEM. Established mathematical models were first developed by Akaret (P-criterion) as a criterion that related pressure in the welding chamber and flow stress of the material as a critical threshold for sound seam weld formation [1]. Plata and Piwinik then later extended on this criterion by integrating P-Criterion over the time of material flow in the weld chamber (Q-criterion) [9]. Donati and Tomesani incorporated effects from seam weld path and contact area (K-criterion) and most recently Yu et al proposed J-criterion accounting for effects from pressure, flow stress, time, and diffusion with a constant applied for surface condition [10, 11]. Researchers have used FEM simulations to explore seam weld in many different porthole-die extrusion applications such as multicavity and complex hollow profiles [12, 13]. While seam weld criterion and FEM show potential in a multitude of weld seam aspects, both are subject to model input and validation by means of physical simulation or extrusion trials.

4. Technology Approach

4.1. Material selection and preparation

Aluminum alloy 6005A was used throughout the investigation for its popular use in the extrusion industry for structural parts in automotive applications. Blanks for physical simulation were machined from direct-chill cast billets homogenized for 4 hours at 560 °C. The precise composition of the alloy is listed in Table 1.

Table 1: AA 6005A Composition by wt%. Aluminum Association composition limits for this alloy are listed for reference [14]

	Si	Fe	Cu	Mn	Mg	Zn	Ti	Cr	Al
6005A	.5 – .9	.35	.30	.50	.40 – .70	.20	.10	.30	Balance
Lot 1	.72	.12	.09	.23	.53	.03	.029	.005	
Lot 2	.80	.12	.10	.25	.57	.02	.003	.005	

The blanks were then machined to 15 mm in length and 10 mm in diameter.

4.2. Physical Simulation

A Gleeble 3500 thermomechanical simulator equipped with stainless steel uniaxial compression anvils was used to simulate temperatures and deformation conditions of porthole extrusion dies. Two blanks were placed between the anvils and were compressed at temperatures of 371, 428, 482, 537 °C and deformation rates of 0.1, 1, 5, and 10 mm/mm/s. Heat rate, compression, compression hold time, and starting temperature were all held constant at 1 °C/s, 109%, 3s, and 20 °C, respectively and samples were air quenched upon release. Additionally, graphite foil was placed at the interface of each sample and anvil to minimize friction that may cause additional strain on the blanks and to reduce the risk of damaging the samples during removal from the Gleeble 3500. The blanks were heated by the Gleeble 3500's direct-resistance heating and temperature was controlled by thermocouples welded 1 mm apart across the blank interface (Figure 1), to ensure symmetrical heating of both blanks. The blanks were then compressed together into a 10 mm sample that was used for tensile testing and microstructural characterization. Flow stress curves were also generated from the resulting stress and strain data output by the Gleeble 3500, and the data was used to accurately model plasticity during DEFORM simulations. Single blank, uniaxial, isothermal compression tests were also performed with the same alloy to validate the flow stress behavior of the novel test with two coupons. Further, some compression samples were machined to 30 mm long x 10 mm in diameter to maintain similar sample dimensions for extracting micro tensile samples on specimens without a weld interface.

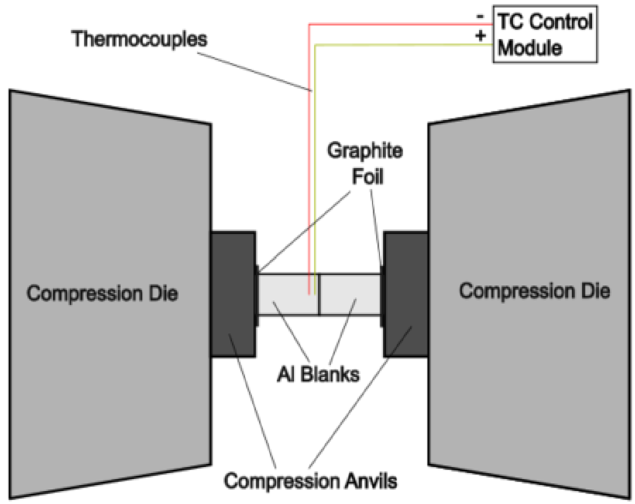

Figure 1: Schematic of physical simulation experimental setup in Gleeble 3500

4.3. Numerical Simulation

To investigate local stress, strain, strain rate, and temperature behavior in the proposed physical simulation technique, DEFORM 2D FEM studies were performed. Studies were performed matching temperature and strain rate conditions used in the physical simulation experiments. Material behavior was modeled using flow stress measurements output from the physical simulation experiments and an Arbitrary Langrangian-Eulerian (ALE) meshing scheme was applied to avoid mesh distortion from large deformation. Further, model symmetry was exploited to reduce computation time. Figure 2, displays the beginning and end of the modeling steps for a 5 s^{-1} strain rate and 537 °C simulation with corresponding mesh (Figures 2a, 2b, 2d, 2e) and strain (Figures 2c and 2f) behavior. From each simulation, local deformation maps were recorded to ensure homogenous deformation between each micro tensile test extracted from the physical simulation experiments.

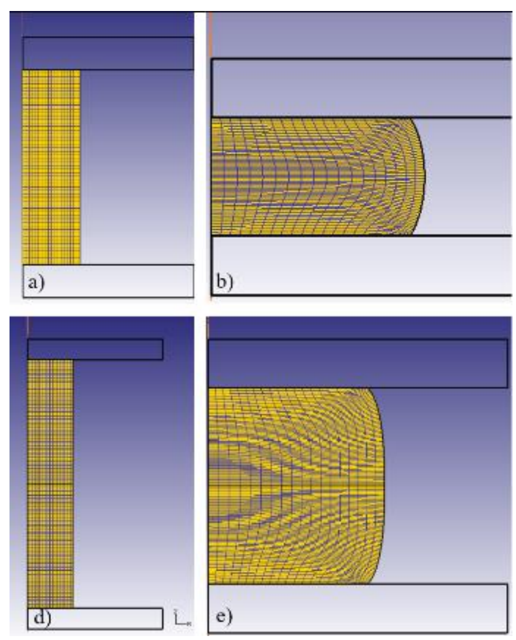

Figure 2: DEFORM 2D start and end step meshes at a strain rate of 5 s^{-1} and temperature of 537 °C for single blank (a and b) and double blank (d and e) compression.

4.4. Mechanical Testing

Micro tensile testing was performed to quantify the effect on bond strength of temperature and strain rate condition by extracting tensile bars from the physical simulation experiments (including reference single blank experiments). To prepare tensile bars from the physical simulation experiments (Figure 3), compressed coupons were milled in a HAAS TM-1 CNC Mill using soft jaws to hold the samples in place during milling. The coupon was first faced to remove 5.4 mm and then geometry of the tensile specimen is milled with a 6.35 mm end mill and a 2.38 mm end mill. After milling a tensile shape with a depth of 6.2 mm, the sample is flipped to produce a square boss of 10mm x 10mm x 5mm for holding in wire electrical discharge machining (EDM) operations. For EDM cutting of the tensile coupons, a skim pass was taken across the sample with the EDM wire to produce parallel cuts. The final tensile coupon is approximately 1.45 mm in thickness, Figure 4 shows the final specimen geometry. The EDM cut samples were surfaced with 400 grit SiC paper to remove the recast layer of the EDM. During tensile testing, the samples were coated with Al_2O_3 powder to produce patterning for digital image correlation (DIC) recognition. The samples are immersed in the powder and shaken lightly. The powder is adhered through electrostatic forces to produce a contrasting image for DIC imaging. Samples were placed in the grips of an Instron screw driven tensile frame and pulled at a constant crosshead rate of 2mm/min. Prior to testing, 2D video image correlation (VIC2D) was set up to capture the strain pattern across the sample and the sample is pulled in the tester till failure.

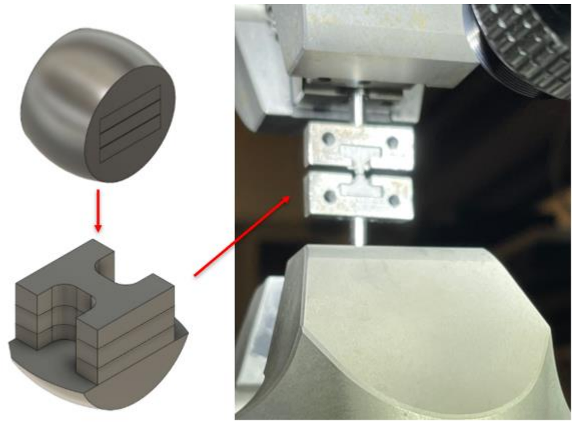

Figure 4: Simplified tensile test machining schematic and tensile bar setup in micro tensile tester

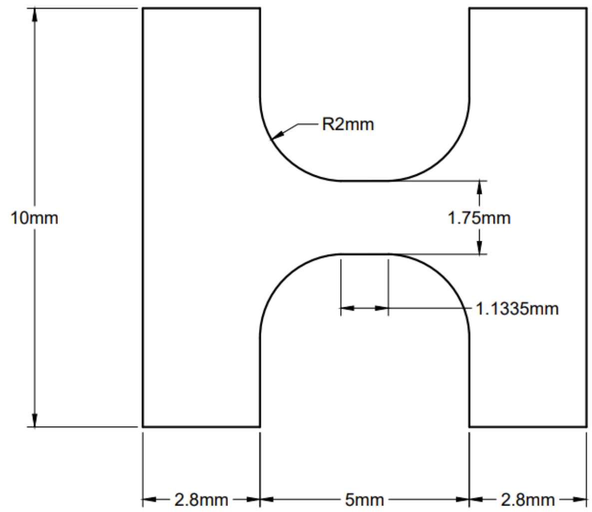

Figure 3: Micro tensile test specimen geometry. Specimen thickness is approximately 1.45 mm.

4.5. Microstructural Characterization

Microstructural characterization was conducted using physical simulation samples sectioned in half and mounted in epoxy-resin and subsequently grinded and polished. Grinding was performed on a Buehler AutoMet250 autopolished with decreasing SiC grinding papers from grits of 320, 400, and 600, respectively. Polishing was then performed with 9, 6, 3, 1 and 0.25 µm diamond suspensions. A final vibratory polish in 0.01 µm colloidal silica for 30 minutes was then performed on a Buehler Vibromet2 vibratory polisher. Light optical microscopy (LOM) using a Zeiss Axiovert 40 MAT optical microscope. Scanning electron microscopy (SEM) and electron backscatter diffraction (EBSD) were carried out using a FEI Scios dual-beam Focused Ion Beam (FIB) equipped with a Shottky field emission gun SEM. Prior to being placed in the chamber, samples were cleaned with ethanol and copper tape was applied to the epoxy resin surface to minimize charging effects in each image. EBSD scans were performed on the same SEM unit with an EDAX Hikari Super EBSD Camera and SEM parameters including a 30 kV accelerating voltage, 6.4 nA beam current, 19 to 20 mm working distance, and a 70° sample tilt to maximize backscatter yield. Dynamic background subtraction was performed on each pattern to accommodate for decreased pattern resolution at the top and bottom of each scan caused by the low magnification on a significant sample tilt. EBSD data was acquired using EDAX Team software and then analyzed using TSL OIM Analysis TM version 8 software. OIM was used to generate inverse pole figure (IPF) maps. EBSD maps were subjected to a grain dilation cleanup procedure.

4.6. Seam Weld Criterion Development

From the resulting micro-tensile tests, a seam weld criterion is proposed based on the elongation of the samples. Solid-state bond formation is characterized by ductile fracture, while poor bond formation is associated with brittle fracture. This is evidenced by Oostekamp et al.'s "kissing" bond phenomenon, where metal surfaces appear bonded in the solid state but are only held together by the friction of the geometrically mated surfaces [15]. Brittle failure of metallic solid-state bonds is also characterized by low tensile strength and rapid fracture, in contrast to ductile failure, which results in a more gradual fracture. This makes brittle failure a dangerous mode in structural applications. Ductile fracture of metals is typically defined as having an elongation of 5% or greater [16]. Therefore, for this investigation, a weld criterion based on the elongation from the micro tests is proposed: bonding onset occurs at 4% elongation, and strong bonding is considered to occur at elongations greater than 5%. Based on this criterion, micro-tensile tests yielding less than 4% elongation are classified as a "fail," those with elongation greater than or equal to 4% but less than 5% as "marginal," and those with elongation greater than or equal to 5% as a "pass."

5. Results and Discussion

5.1. Physical Simulation Results

Figure 5 provides flow stress data for samples tested at different temperatures. As temperature decreases, a significant increase in flow stress is observed. A similar trend was found with deformation where increasing strain rate resulted in an increase in flow stress. This relationship closely follows that described by the Sellars-McTegart model and results from Shi et al for the same aluminum alloy [17, 18]. A max flow stress in Figure 5 of approximately 90 MPa and a minimum flow stress of 40 MPa were both found, exhibiting that this physical simulation technique can cover a broad range of extrusion flow stresses. Further, comparison with isothermal compression tests with one blank (represented by the dashed lines in Figure 5) show little deviation proving that accuracy of the output flow stress data is not lost by the novelty of the technique.

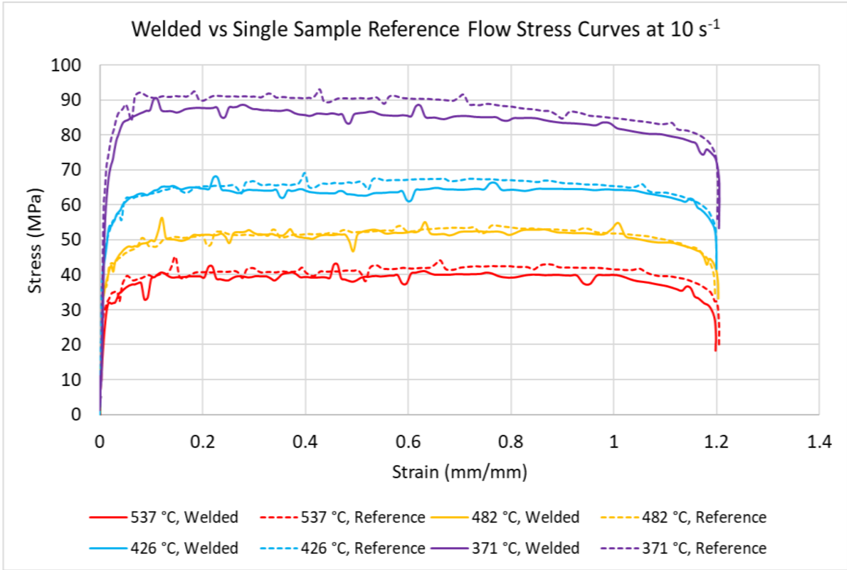

Figure 5: Resulting flow stress curves from physical simulation performed at a 10 s^{-1} strain rate. Single sample reference curves are also plotted to compare accuracy of the physical simulation flow stress measurements.

5.2. Numerical Simulation Results

The strain map shown in Figure 6 exhibits symmetrical, uniform deformation in the specimen extraction area. The same symmetry was found for all physical simulation conditions, only differing in magnitude. Provided the sample thickness and gauge length dimensions described by Figure 4, extraction of three micro tensile samples from the physical simulation experiments is theoretically possible. Extracting three samples per experiment will allow for better control of statistical accuracy and efficiency of the technique as a whole.

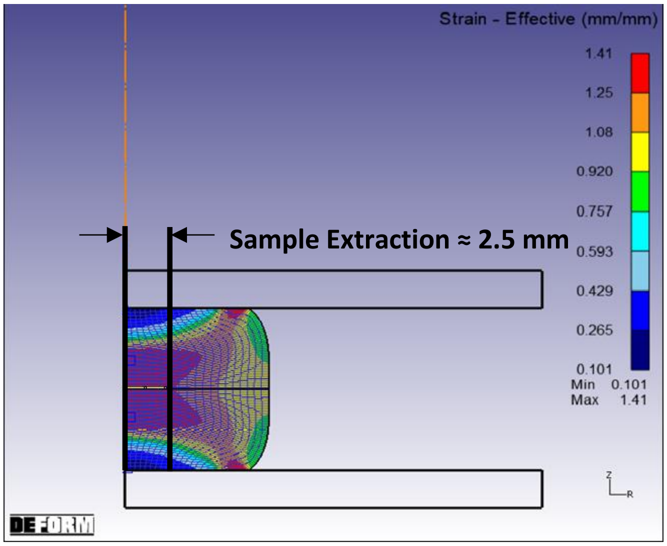

Figure 6: FEM local strain map resulting from simulation conditions of 537 °C and 0.1 s^{-1}

5.3. Mechanical Testing Results

From the micro tensile testing, relationships between physical simulation strain rate and bond strength and ductility can be made. Table 2 displays the resulting average ultimate tensile strength (considered as bond strength) and

Table 2: Resulting average ultimate tensile strengths and elongation at fracture and weld acceptance of micro tensile testing.

Temperature (°C)	Strain Rate (s^{-1})	Average Ultimate Tensile Strength (MPa)	Average Elongation (%)	Acceptance
371	0.1	N/A	N/A	Fail
371	1	151 ± 15	5.8 ± 1.2	Pass
371	5	128 ± 46	8.9 ± 3.9	Pass
371	10	173 ± 2	10.5 ± 1.1	Pass
426	0.1	N/A	N/A	Fail
426	1	N/A	N/A	Fail
426	5	N/A	N/A	Fail
426	10	102 ± 45	5.6 ± 2.4	Pass
482	0.1	107± 17	2.8 ± 0.4	Fail
482	5	169 ± 20	5.2 ± 1.0	Pass
482	10	215 ± 2	10.8 ± 0.7	Pass
537	0.1	162 ± 21	3.9 ± 0.8	Marginal
537	1	52 ± 2	1.8 ± 0.1	Fail
537	5	95 ± 24	3.1 ± 0.5	Fail
537	10	187 ± 24	7.2 ± 2.8	Pass

elongation. Discrepancies between tests under the same physical simulation conditions are observed, with significant errors in some of the tests. The origin of these discrepancies is due to misalignment of the cylindrical blanks during hot compression. Misalignment during compression shifts the local deformation conditions, resulting in an asymmetrical deformation gradient, as opposed to the desired symmetrical deformation gradient shown in Figure 6. Additionally, samples with very poor bonding conditions, such as those tested at 371 °C and a strain rate of 0.1 s^{-1}, failed before tensile force could be applied and were considered to have no elongation. The results show a maximum bond strength of 214.8 MPa and an elongation of 10.8% under physical simulation conditions of 482 °C and a strain

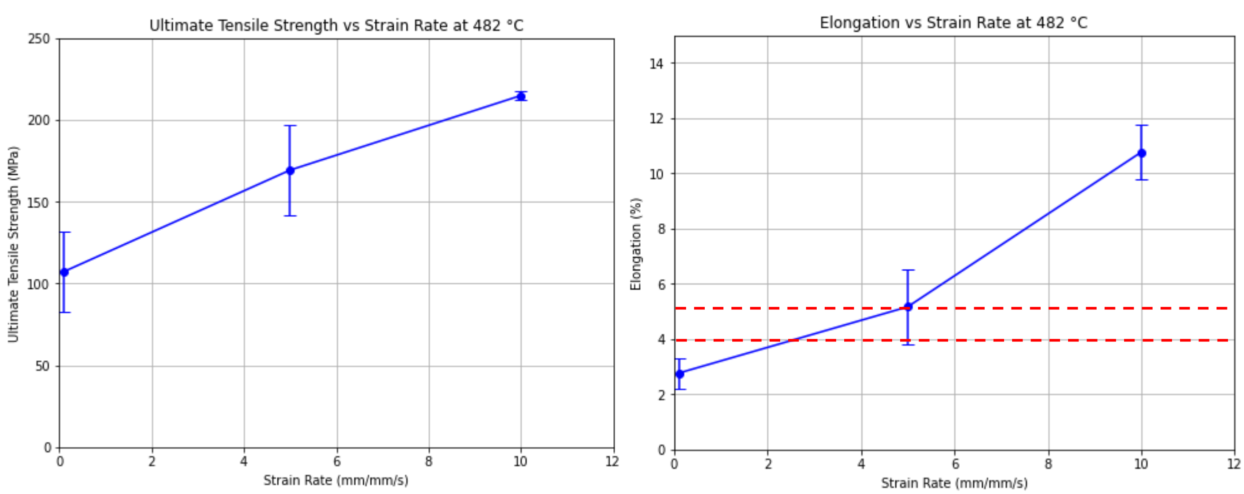

Figure 7: Average ultimate tensile strength (left) and elongation (right) with physical simulation strain rate for compression at 482 °C. Dashed red lines indicate the limits for fail, marginal and passing elongation criteria.

rate of 10 s⁻¹. Despite data discrepancies in Table 2, a relationship between physical simulation strain rate and bond quality can be established. For each compression temperature, a significant improvement in bond strength and elongation is observed with an increasing compression strain rate. This relationship is demonstrated in Figure 7 for samples compressed at 482 °C. From Figure 7, a nearly linear relationship between both bond strength and elongation can be observed. At other temperatures, linearity is not present, but an increase in bond quality is still noted with a higher strain rate.

Weld acceptance is also shown in Table 2 and Figure 7. In Table 2, seven out of 15 combinations of physical simulation conditions passed the proposed criterion. Among the conditions that passed, compression at 482 °C and 10 s⁻¹ resulted in the best bond quality. This result demonstrates how users of this physical simulation method can repeat experiments under different processing/alloy conditions to determine the minimum and optimal conditions for sound seam weld formation. Furthermore, by generating plots similar to the one in Figure 7, users can efficiently optimize process conditions using minimal material and avoid process scrap generated by trial extrusions.

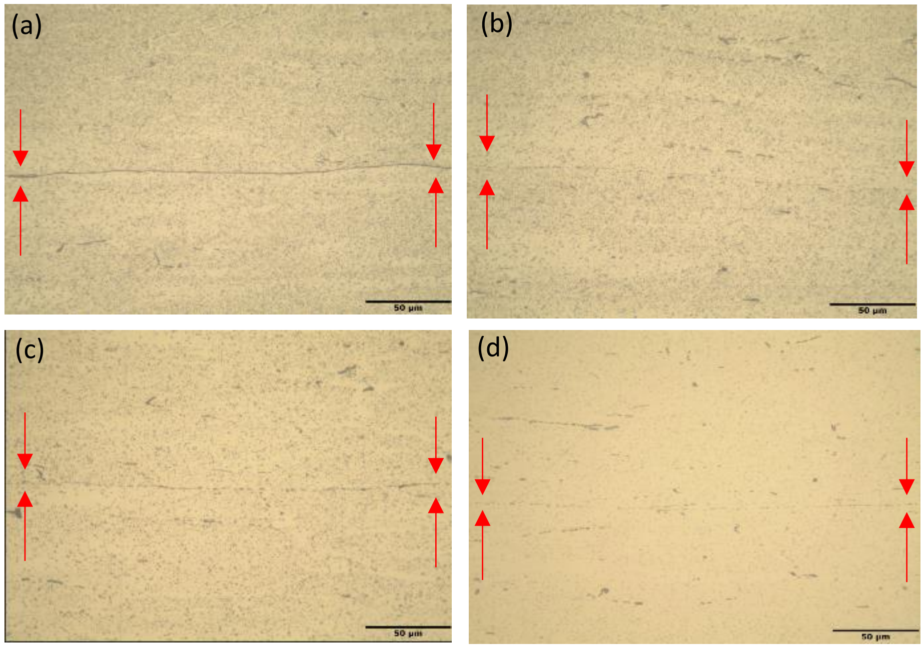

Figure 8: LOM images of the 0.1 s^{-1} (a and c) and 10 s^{-1} (b and d) and 371 °C (a and b) and 537 °C (c and d) physical simulation experiments. Red arrows indicate the lateral extremities of the bond line in each micrograph.

5.4. Microstructural Characterization

From the light optical micrographs in Figure 8, bond interface propagation is observed. In Figure 8a, the interface is completely continuous along its full length, with minimal bond sites. In contrast, Figure 8d depicts a highly fragmented interface with a large number of bond sites. The increase in bond locations helps explain the relationship between strain rate and bond quality observed in Table 2 and Figure 7. An increased global strain rate leads to faster fracture and evacuation of oxides trapped at the interface, resulting in a larger number and size of bond sites. To better understand the underlying mechanism responsible for the increased bond strength under higher strain rate conditions, an EBSD scan of the weld interface shown in Figure 8c was performed, and the IPF map in Figure 9 was generated. Figure 9 reveals recrystallized grains at the weld interface, which is characteristic of the onset of bond formation according to the Recrystallization Theory of Solid-State Bonding [19]. The

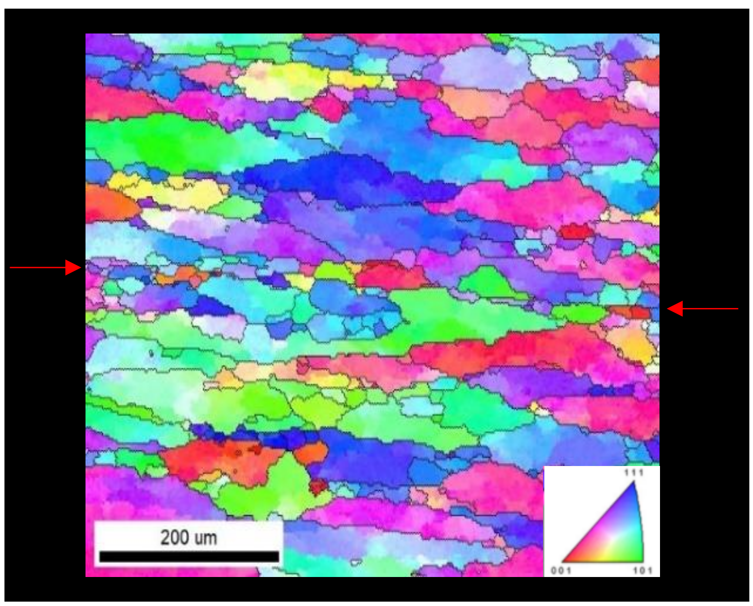

Figure 9: EBSD IPF map of 0.1 s^{-1}, 537 °C physical simulation experiment bond region. Red arrows indicate where the bond line occurs.

elongation of the sample observed in Figure 9 is 3.9 ± 0.8%, as per Table 2, just short of the bond formation threshold according to the proposed criterion. This result aligns well with the minimal recrystallization present at the weld interface, as dynamic recrystallization responsible for bond formation is a temperature- and deformation-dependent process [20]. Despite the lower deformation rate, the elevated temperature in this instance still promotes the best bonding conditions compared to other temperatures at a strain rate of 10 s^{-1}.

6. Conclusions & Recommendations

This report investigates an improved physical modeling method to simulate solid-state bonding mechanisms in porthole-die extrusion seam welds. The following conclusions can be drawn from the described investigation:

- A novel method for physically simulating solid state welds under different conditions of strain rate, temperature and time was presented. To the author's knowledge, this is the first physical simulation using a Gleeble device to simulate seam weld conditions under isothermal conditions. Further, micro mechanical testing of coupons taken across the weld interface is a valuable tool for measuring the integrity of the welds.
- Different levels of bonding and mechanical properties were observed when comparing samples from different thermomechanical testing parameters. Resulting micro tensile data suggests increased strain rate has the most positive influence on weld acceptance.
- A criterion based on micro tensile test elongation was developed. Extruders can use this criterion combined with the physical simulation experiments to determine seam weld acceptance based on local temperature and strain rate conditions in the porthole die welding chamber. This in turn can be used to reduce process scrap generated by trial extrusions performed to asses seam weld quality by preliminarily rejecting process conditions that will yield poor seam weld formation.

Future work is focused on integrating the physical simulations into numerical simulations of the extrusion process to predict the integrity of the weld joints. Additionally, full scale extrusion trials will be performed to evaluate the effectiveness of the acceptance criterion developed.

7. Acknowledgements

The authors of this manuscript would like to acknowledge the DOE and the REMADE institute for funding this work.

8. References

1. Akaret, R., Properties of pressure welds in extruded aluminum alloy sections, J. Inst. Met., 100, 202-208, 1972.

2. Kazakov, N.F., A Diffusion Bonding of Materials, Pergamon Press, pp. 17-48, 1980.

3. Swiatkowski, K., Physical modelling of metal working processes using wax-based model materials, J. Met. Proc. Tech., 72, 2, 272-276, 1997.

4. Holmquist, J.L., Investigation of the piercing process by means of model wax billets, Iron Steel Eng., 53-68, 1952.

5. Chakkingal, U., Misiolek, W.Z., Microstructure characterization of extrusion welding in a magnesium alloy extrudate, in: Proc. of 1998 TMS Annual Meeting, Minerals, Met., and Mater. Soc., pp. 195-205, 1998.

6. Edwards, S.P., Den Bakker, A.J., Zhou, J., Katgerman, L., Physical simulation of longitudinal weld seam formation in aluminum extrusions, JSME Int. J., 49(1), 63-68, 2006.

7. Cooper, D.R., Allwood, J.M., The influence of deformation conditions in solid-state aluminum welding processes on the resulting weld strength, J. Mater. Proc. Tech., 214, 11, 2576-2592, 2014.

8. Bai, S.W., Fang, G., Zhou, J., Analysis of the bonding strength and microstructure of AA6082 extrusion weld seams formed during physical simulation, J. Mater. Process. Technol., 250, 109-120, 2017.

9. Plata, M., Piwnik, J., Theoretical and experimental analysis of seam weld formation in hot extrusion of aluminum alloys, in: Proc. 7th Int. Aluminum Extrusion Tech. Seminar, pp. 205-211, 2000.

10. Donati, L., Tomesani, L., The prediction of seam welds quality in aluminum extrusion, J. Mater. Proc. Tech., 153, 366-373, 2004.

11. Yu, J., Zhao, G., Chen, L., Analysis of longitudinal weld seam defects and investigation of solid-state bonding criteria in porthole die extrusion process of aluminum alloy profiles, J. Mater. Proc. Tech., 237, 31-47, 2016.

12.Chen, H., Zhao, G.Q., Zhang, C.S., Guan, Y.J., Liu, H., Kou, F.J., Numerical simulation of extrusion process and die structure optimization for a complex aluminum multicavity wallboard of high-speed train, Mater. Manuf. Process., 26, 1530-1538, 2011.

13. Den Bakker, A.J., Weld Seam in Aluminum Alloy Extrusion: Microstructure and Properties, Doctoral thesis, Delft University of Technology, 2016.

14. Standard specification for AA6005A chemical composition limits, The Aluminum Association, 2018.

15. Oosterkamp, A., Oosterkamp, L., Nordeide, A., Kissing bond phenomena in solid-state welds of aluminum alloys, Welding J., 83, 225-231, 2004.

16. Astakhov, V.P., Mechanical Properties of Engineering Materials: Relevance in Design and Manufacturing, in: Davim, J. (Ed.), Introduction to Mechanical Engineering. Materials Forming, Machining and Tribology, Springer, Cham, pp. 1-10, 2018.

17. Sellars, C.M., McTegart, W.J., On the mechanism of hot deformation, Acta Metall., 14, 1136-1138, 1966.

18. Shi, L., Yang, H., Guo, L.G., Zhang, J., Constitutive modeling of deformation in high temperature of a forging 6005A aluminum alloy, Mater. & Design, 54, 576-581, 2014.

19. Parks, J., Recrystallization welding, Weld. Res. Suppl., 32, 209-222, 1953.

20. Huang, K., Logé, R.E., A review of dynamic recrystallization phenomena in metallic materials, Mater. & Design, 111, 548-574, 2016.

About the Authors

Roni J. Rountree is a doctoral student in materials science and engineering at Lehigh University. He is a member of the Loewy Institute and specializes in metallurgy of aluminum alloys and physical modeling of extrusion.

Charles C. Yurgel is a postdoctoral researcher of materials science and engineering department at Lehigh University. His expertise involves evaluation of metal forming with numerical process simulation and physical material modeling that enable new developments for the industry.

Nicholas E Nanninga is the General Manager at Secat, Inc. His research interests are focused on alloy and process development for commercial applications.

Randall L. Bowers focuses on the field of aluminum rolling ingot for beverage can sheet and automotive alloys. He handles projects related to failure analysis, product development, mechanical testing, modeling, thermodynamic calculations, heat treating, DIC strain analysis, and microscopy.

Paul F. Rottmann is an assistant professor of materials engineering at the University of Kentucky. He has extensive expertise in the mechanical and microstructural characterization of structural materials including aluminum alloys, additively manufactured metals, and refractory composites.

Wojciech Z. Misiolek is the Loewy Professor in the Department of Materials Science and Engineering and the Director of the Loewy Institute at Lehigh University in Bethlehem, PA, USA. His main research focus is on optimizing the processing of metals and alloys.